

University of Nebraska - Lincoln

DigitalCommons@University of Nebraska - Lincoln

---

School of Natural Resources: Faculty  
Publications

Natural Resources, School of

---

2023

## Contrasting photoprotective responses of forest trees revealed using PRI light responses sampled with airborne imaging spectrometry

J. A. Gamon

*University of Nebraska - Lincoln*

R. Wang

*University of Nebraska - Lincoln*

Sabrina E. Russo

*University of Nebraska - Lincoln*, [srusso2@unl.edu](mailto:srusso2@unl.edu)

Follow this and additional works at: <https://digitalcommons.unl.edu/natrespapers>



Part of the [Natural Resources and Conservation Commons](#), [Natural Resources Management and Policy Commons](#), and the [Other Environmental Sciences Commons](#)




---

Gamon, J. A.; Wang, R.; and Russo, Sabrina E., "Contrasting photoprotective responses of forest trees revealed using PRI light responses sampled with airborne imaging spectrometry" (2023). *School of Natural Resources: Faculty Publications*. 1712.  
<https://digitalcommons.unl.edu/natrespapers/1712>

This Article is brought to you for free and open access by the Natural Resources, School of at DigitalCommons@University of Nebraska - Lincoln. It has been accepted for inclusion in School of Natural Resources: Faculty Publications by an authorized administrator of DigitalCommons@University of Nebraska - Lincoln.

## Methods

## Contrasting photoprotective responses of forest trees revealed using PRI light responses sampled with airborne imaging spectrometry

John A. Gamon<sup>1</sup> , Ran Wang<sup>1</sup>  and Sabrina E. Russo<sup>2,3</sup> <sup>1</sup>School of Natural Resources, University of Nebraska-Lincoln, Lincoln, NE 68583-0961, USA; <sup>2</sup>School of Biological Sciences, University of Nebraska-Lincoln, Lincoln, NE 68588-0118, USA; <sup>3</sup>Center for Plant Science Innovation, University of Nebraska-Lincoln, Lincoln, NE 68588-0660, USA

Authors for correspondence:

John A. Gamon

Email: [jgamon@unl.edu](mailto:jgamon@unl.edu); [jgamon@gmail.com](mailto:jgamon@gmail.com)

Received: 5 June 2022

Accepted: 16 January 2023

New Phytologist (2023) 238: 1318–1332

doi: 10.1111/nph.18754

**Key words:** airborne remote sensing, carotenoid pigments, drought, environmental stress, imaging spectrometry, Photochemical Reflectance Index (PRI), xanthophyll cycle.

## Summary

- The Photochemical Reflectance Index (PRI) provides an optical indicator of photosynthetic light-use efficiency, photoprotection, and stress in plants. Although PRI can be applied in remote sensing, its interpretation depends on irradiance, which is hard to obtain from satellite or airborne imagery.
- To quantify forest photoprotective responses remotely, we developed a framework for modeling and interpreting PRI-light responses of individual trees and species using airborne imaging spectrometry coupled with georeferenced forest inventory data from a temperate broad-leaved forest. We derived an irradiance proxy, used hierarchical modeling to analyze PRI-light responses, and developed a framework of physiological interpretations of model parameters as facultative and constitutive components of photoprotection.
- Photochemical Reflectance Index declined with illumination, and PRI-light relationships varied with landscape position and among tree crowns and species. More sun-exposed foliage had lower intercepts and slopes of the relationship, indicating greater constitutive, but less facultative, photoprotection.
- We show that tree photoprotective strategies can be quantified at multiple scales using airborne hyperspectral data in structurally complex forests. Our findings and approach have important implications for the remote sensing of forest stress by offering a new way to assess functional diversity through dynamic differences in photoprotection and photosynthetic downregulation and providing previsual indicators of forest stress.

## Introduction

The Photochemical Reflectance Index (PRI), a reflectance-based index of plant photoprotective pigment responses to environmental conditions (Gamon *et al.*, 1992), has been widely used as an optical metric of dynamic photosynthetic regulation (Garbalsky *et al.*, 2011; Zhang *et al.*, 2016). Many traditional reflectance-based vegetation indices sample plant characteristics related to slowly changing green canopy structure (e.g. the Normalized Difference Vegetation Index, NDVI). By contrast, PRI responds to changes in carotenoid pigments tied to photosynthetic light energy distribution and is affected by multiple environmental factors affecting photosynthetic processes, principally illumination (Gamon *et al.*, 1992), but also including vegetation water status (Asner *et al.*, 2004; Peguero-Pina *et al.*, 2008; Suarez *et al.*, 2008; Damm *et al.*, 2022), nutrient status (Peñuelas *et al.*, 1994; Gamon *et al.*, 1997), temperature (Wong & Gamon, 2015), and disease (Feng *et al.*, 2017).

Over diurnal timescales, when illumination and other environmental conditions may be changing rapidly, variation in PRI of leaves and canopies reflects the operation of the xanthophyll cycle (Gamon *et al.*, 1990, 1992, 1997), which dissipates excess absorbed light energy as heat during conditions unfavorable for carboxylation (Demmig-Adams & Adams, 1996, 2000). On these short timescales, PRI is closely tied to reversible nonphotochemical quenching (NPQ) of chlorophyll fluorescence (Gamon *et al.*, 1997; Peguero-Pina *et al.*, 2008; Alonso *et al.*, 2017; Vilfan *et al.*, 2019; Wang *et al.*, 2020) and provides an indicator of photosynthetic light-use efficiency (Gamon *et al.*, 1992; Peñuelas *et al.*, 1995). Over longer temporal scales, variation in PRI is also strongly influenced by the relative levels of carotenoid and chlorophyll pigments (Sims & Gamon, 2002; Garrity *et al.*, 2011; Gamon & Berry, 2012), providing an indicator of seasonal photosynthetic regulation and gross primary productivity (GPP) (Wong & Gamon, 2015) likely related to sustained NPQ (*sensu* Demmig-Adams & Adams, 2006). These short- and long-term

PRI pigment effects have been called ‘facultative’ and ‘constitutive’ responses, respectively (Gamon & Berry, 2012). Both involve photosynthetic and photoprotective pigments but represent distinct mechanisms operating over different temporal scales (Sims & Gamon, 2002; Filella *et al.*, 2009; Gamon *et al.*, 2015). By capturing the capacity of plants for both rapid adjustments in xanthophyll cycle activity and slower variation in photoprotective pigment pools, quantifying *both* facultative and constitutive variation in PRI enhances the ability to distinguish functional variation in photosynthetic and photoprotective responses under dynamic environmental conditions.

Plant species and functional groups often differ in their PRI behavior (Gamon *et al.*, 1997; Garbulsky *et al.*, 2011; Kothari *et al.*, 2018), presumably reflecting various strategies for coping with excess light. A study in a boreal forest using airborne imaging spectrometry found that species-mapping approaches that were partly based on PRI and relative pigment levels performed well against other classification methods (Fuentes *et al.*, 2001), suggesting that variation in PRI-light responses can reveal species’ differences in photosynthetic and photoprotective functions in complex landscapes. A wide range of photoprotective strategies, encompassing fluorescence, PRI, leaf movements, and leaf shedding have been observed in functionally diverse tropical forest stand (Gamon *et al.*, 2005). Like many spectral vegetation indices, PRI is also strongly influenced by illumination and canopy structure (Barton & North, 2001; Gitelson *et al.*, 2017). Canopy regions varying in light exposure have contrasting PRI-light responses reflecting their recent light histories associated with canopy position but also their instantaneous light environments (Gamon *et al.*, 2005; Gamon & Berry, 2012; Atherton *et al.*, 2017; Schmiede *et al.*, 2022). Adjacent trees of different height and contrasting hydraulic conductance and stomatal conductance exhibit different PRI-light responses, indicating more photosynthetic downregulation in taller trees (Gamon & Bond, 2013). These findings indicate that variation in canopy PRI-light responses can reveal adaptive variation between species in their photosynthetic and photoprotective functions.

The Photochemical Reflectance Index has the potential to be a powerful and informative indicator of the responses of vegetation to environmental stressors, such as caused by drought, nutrient deficiency, and temperature extremes. This ability of PRI is now being proposed in precision agriculture to improve irrigation management (Wong *et al.*, 2022) and is also useful in phenotyping (Machwitz *et al.*, 2021). The ability to detect early, previsual stress over large spatial and temporal scales with remote sensing may provide early warning indicators of incipient vegetation dysfunction that could eventually lead to stand-level compositional changes. However, the variability of PRI also complicates its interpretation, particularly in complex landscapes, when contextual information about environmental conditions, particularly irradiance, is lacking. The effects of an individuals’ light environment and its canopy structure add complexity to the interpretation of PRI (Barton & North, 2001), particularly when both vary across time and space, as typically happens in natural landscapes. Therefore, to effectively apply remotely sensed PRI as a previsual

indicator of vegetation stress, it is helpful to quantify the PRI-light relationship. Contrasting PRI-light responses offer a valuable tool to recognize conditions of vegetation stress and identify individuals and species that are particularly vulnerable to environmental stressors.

Accounting for illumination has often been done in ground-based studies of PRI at leaf, crown, and stand scales (Gamon & Surfus, 1999; Hall *et al.*, 2008; Hilker *et al.*, 2008; Gamon & Berry, 2012; Gamon & Bond, 2013; Hmimina *et al.*, 2014; Magney *et al.*, 2016). In these cases, PRI declined with increasing illumination, with the degree of decline indicating the degree of excess absorbed light, the degree of photosynthetic downregulation, and the integrated effects of various stressors on the photosynthetic system (Gamon, 2015). At the leaf-scale, it is relatively simple to measure PRI on dark-adapted leaves ( $PRI_0$ ), then observe the change in PRI with increasing illumination ( $\Delta PRI$ ), providing PRI-light response curves that can reveal dynamic xanthophyll cycle activity and photosynthetic downregulation in response to stress.  $\Delta PRI$  and  $PRI_0$  can also distinguish the short-term xanthophyll cycle activity (the facultative response) from the long-term pigment pool-size effects (the constitutive response), respectively (Gamon & Berry, 2012; Hmimina *et al.*, 2014; Magney *et al.*, 2016). However, to our knowledge, these methods of analyzing the PRI-light response have not yet been applied in aircraft or satellite remote sensing campaigns, which often involve a single overpass under particular illumination conditions (typically full sun near midday).

In this study, our goal was to evaluate within and between species variation in photoprotective responses in a complex forest stand by quantifying differences in the PRI-light response in heterogeneous, mixed-species forested landscapes from airborne imaging spectrometry. We developed an approach to quantifying the PRI-light responses at the individual tree and species scales by coupling hyperspectral imagery with data from a fully georeferenced forest inventory plot. Because direct, independent assessment of dynamic illumination and photosynthetic behavior of top-canopy foliage was not possible due to the lack of canopy access, as is typically the case for forest stands, we assessed crown illumination by developing a pixel-level irradiance proxy based on apparent canopy albedo in the photosynthetically active radiation (PAR) range (400–700 nm). To ascribe relative contributions of illumination, as well as individual and species-level variation to the PRI responses, we developed a hierarchical modeling approach that accounts for these nested sources of variation in the measured PRI. Intercept and slope parameters estimated from this model allowed us to derive remote-sensing-based metrics of the PRI-light relationship corresponding to the  $PRI_0$  and  $\Delta PRI$  of ground-based studies, enabling more informative physiological interpretations of variation in remotely sensed PRI. Using model selection, we tested the hypothesis that accounting for light-dependent variation in PRI would enable us to distinguish variation in PRI-light responses among individuals and species and thereby detect differences in photoprotection. We predicted that PRI would decrease with greater illumination and that the overall variation in the PRI-light relationship would be further structured by functional differences within and among



individual tree crowns, across species, and with landscape position.

## Materials and Methods

### Study site and forest inventory plot

Our study forest, the 18.4-ha Indian Cave forest dynamics plot (ICP) (40.247°N, 95.537°W), is located in Indian Cave State Park, Richardson County, NE, USA. The Park is classified as a Biologically Unique Landscape by the Nebraska Game and Parks Commission (Schneider *et al.*, 2011). Mean annual temperature is 11.2°C (range of monthly averages, −3.2–25.0°C), and cumulative annual rainfall is 875.5 mm (range of monthly accumulation, 10.4–98.6 mm), based on monthly averages of daily, 5-km gridded data for Richardson County, NE, for 1981–2010 from the University of Nebraska High Plains Regional Climate Center ([hprcc.unl.edu](http://hprcc.unl.edu)). The ICP is located on the bluffs, escarpments,

and valleys along the Missouri River (Fig. 1a,b) and is topographically complex with an average elevation of 315 m (range, 276–371 m) (Fig. 1c,d). Soils are well-drained silty loams formed from calcareous loess, becoming more silty-clayey in bottomland alluvium in the lowest elevations (Elder, 1969; Joeckel *et al.*, 2019; Soil Survey Staff, 2021). Bluffs are 1–5-m-thick Preoria Loess overlaying Indian Cave Sandstone or Falls City limestone of the Upper Pennsylvanian System (Elder, 1969; Fischbein *et al.*, 2009). The dominant biome of this region is grassland (prairie), but forests often predominate near rivers, where water is more available (Weaver, 1965).

The dimensions of the ICP are 400 m × 460 m, and it has been gridded with georeferenced markers every 20 × 20 m placed by a professional surveyor. Woody stems (trees, shrubs and lianas) within the ICP were inventoried from July to December, 2019, following standardized protocols (Condit, 1998) of the Smithsonian Forest Global Earth Observatory (ForestGEO) global network of forest dynamics plots (Davies *et al.*, 2021), of

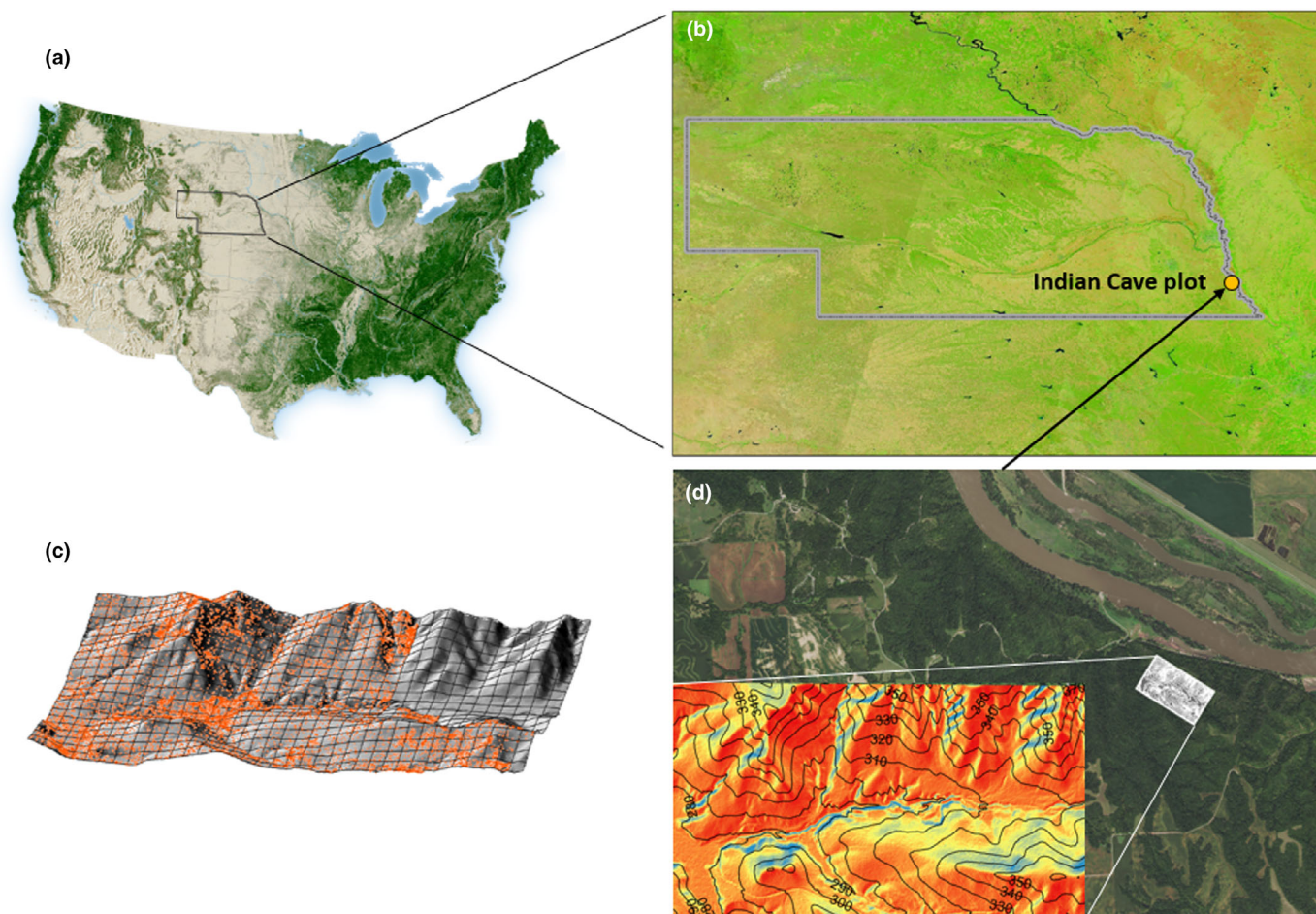


**Fig. 1** Location of the Indian Cave forest inventory plot (ICP) in Nebraska, USA. (a) Location of Nebraska with respect to a map of forest cover in the United States (taken from the US Forest Service's online Forest Atlas of the United States) and (b) a Moderate Resolution Imaging Spectroradiometer (MODIS surface Reflectance 8-Day L3 Global 250m (MOD09Q1) on 15 September 2019) image of the region (Vermote, 2015). In (c), a map of all individual georeferenced woody stems (orange dots) in the Indian Cave plot is overlaid on a hill-shade digital elevation model (DEM; USGS, 2017), and in (d), the location of Indian Cave plot is shown as a contour map in white, on an aerial image (USDA, 2018) of Indian Cave State Park (the Missouri River is visible in the top-right portion of the image) with an inset in the bottom left showing variation in cumulative annual incident solar radiation estimated based on the DEM (the red-yellow-blue color ramp corresponds to declining solar radiation).

which the ICP is a part. Specifically, woody stems  $\geq 1$  cm in trunk diameter at breast height (DBH) have been individually tagged with a unique identification number, identified to species, measured for DBH and condition variables, and assessed for crown exposure (for free-standing stems). Crown exposure was estimated following Clark & Clark (1992) using an index on a scale of 1–5 (1, crown completely shaded; 2, crown receiving  $< 10\%$  direct overhead illumination; 3, crown receiving 10–90% direct overhead illumination; 4, crown receiving  $\geq 90$ , but  $< 100\%$ , direct overhead light; 5, completely sun-exposed crown). Tree trunks were mapped to the nearest  $\approx 20$  cm using a total station (Leica FlexLine plus TS06; Leica Geosystems, St Gallen, Switzerland) referencing the surveyed grid markers. Fifty-nine additional  $20 \times 20$  m quadrats (2.36 ha) outside of the contiguous plot area have also been inventoried, for a total of 16 894 georeferenced trees (Fig. 1c) of 47 woody species in a total of 20.76 ha (Supporting Information Table S1). We extracted the elevation of each tree using a 1-m bare earth digital elevation model (DEM) provided by the US Department of Agriculture (USGS, 2017), which was also used to determine hill-slope irradiance (Fig. 1).

### Airborne data collection and processing

Airborne imagery for the Indian Cave ForestGEO plot was collected at 11:00 h local time on 6 September 2019, using the Nebraska Earth Observatory (NEO), which includes an imaging spectrometer (AISA Kestrel; Specim, Oulu, Finland) mounted on a fixed-wing aircraft (Piper Saratoga; Piper Aircraft, Vero Beach, FL, USA). The imaging spectrometer collected uncalibrated radiance (digital numbers, DN) with a spectral resolution of 2.4 nm full width half maximum (FWHM) at 3.4 nm spectral sampling intervals (178 bands total) from 400 to 1000 nm. The field of view (FOV) was  $40^\circ$ . The image was collected from  $\approx 1500$  m above the ground level and the ground pixel size (IFOV) was  $\approx 1$  m.

Lab-measured calibration coefficients were used to radiometrically convert DN values to at-sensor radiance ( $\text{W m}^{-2} \text{sr}^{-1} \text{nm}^{-1}$ ). Georeferencing was performed utilizing the position and rotational attributes of the airplane collected by an inflight GPS and inertial measurement unit (IMU) (RT3000; Oxford Technical Solutions Ltd, Bicester, UK). Both radiometric calibration and georeferencing were performed using the CALI GEO PRO software package (Specim).

To obtain a corrected surface reflectance of the airborne data, we applied a hybrid atmospheric correction by applying ground measured reflectance of four calibration targets to the MODTRAN 5 (Berk *et al.*, 2008) radiative transfer model outputs. Ground reflectance of four (white, silver, charcoal, and black) calibration targets (Odyssey; Marlen Textiles, New Haven, MO, USA) were collected using a dual channel system by combining two field spectrometers (USB2000; Ocean Optics, Delray Beach, FL, USA) during the flight time. Image data of  $3 \times 3$  pixels from the middle of each of the four ground calibration targets were extracted to avoid any possible target edge effects. We then incorporated the mean surface reflectance of each of the four

calibration targets via Bayesian inference to the MODTRAN outputs (Thompson *et al.*, 2016) to derive surface reflectance as described in Wang *et al.* (2021).

### Irradiance estimation

To determine irradiance for each tree crown pixel in the portion of the image encompassing the ICP, we developed a proxy measure of irradiance. We first calculated the radiance of tree crowns by integrating the measured surface reflectance between 400 and 700 nm (i.e. photosynthetically active radiation, PAR), obtained from the imaging spectrometer to derive an *apparent* PAR albedo, which we refer to as 'PAR albedo'. This calculation assumes that the radiance (amount of reflected radiation detected from tree crowns as measured by the airborne imaging spectrometer) provides a proxy for the incident radiation (irradiance) over this spectral range. This assumption was tested by applying different scenarios of illumination (diffuse vs direct sunlight) and comparing the irradiance to the PAR albedo. The strong linear relationship between irradiance and PAR albedo ( $R^2 = 0.78$ –1 for the different illumination scenarios and canopy reflectance values tested) supported the use of PAR albedo as a pixel-level irradiance proxy (Figs S1, S2). A detailed explanation of this method is provided in Methods S1. We then used this proxy (PAR albedo) to examine the PRI-light response for all pixels associated with an identified tree crown, as described below.

### Analytical framework

We developed a multistep analytical framework (Fig. 2) that combined the data from the fully georeferenced ICP with data from the airborne platform. This analysis evaluated PRI-light responses (using PAR albedo) and considered variation in remotely sensed PRI due to both facultative (shorter-term) and constitutive (longer-term) responses of xanthophyll cycle activity.

### Integrating remote-sensing and forest inventory data to identify tree crowns

We assigned pixels to tree crowns by integrating the airborne data with the ICP forest inventory data. First, we segmented the hyperspectral image by applying a multiresolution image segmentation to delineate different tree crowns using ECOGNITION software (Trimble Inc., Sunnyvale, CA, USA). Image segmentation partitions pixels in a digital image into segments (also known as image objects). The goal was to assign labels to pixels that share certain characteristics and thereby define individual tree crowns. Second, we manually identified 519 segments from the segmented image based on the locations of canopy trees (canopy exposure index  $\geq 4$  and DBH  $\geq 10$ ) in the forest inventory data. We used these data to train a support vector machine (SVM) classifier using the *fitcsvm* function in MATLAB (2020), which used a 10-fold cross-validation and yielded an initial accuracy of 94% when checked against the field-verified identities of exposed canopy trees. This classifier was then applied to the whole image to identify segments with similar spectral properties as those in



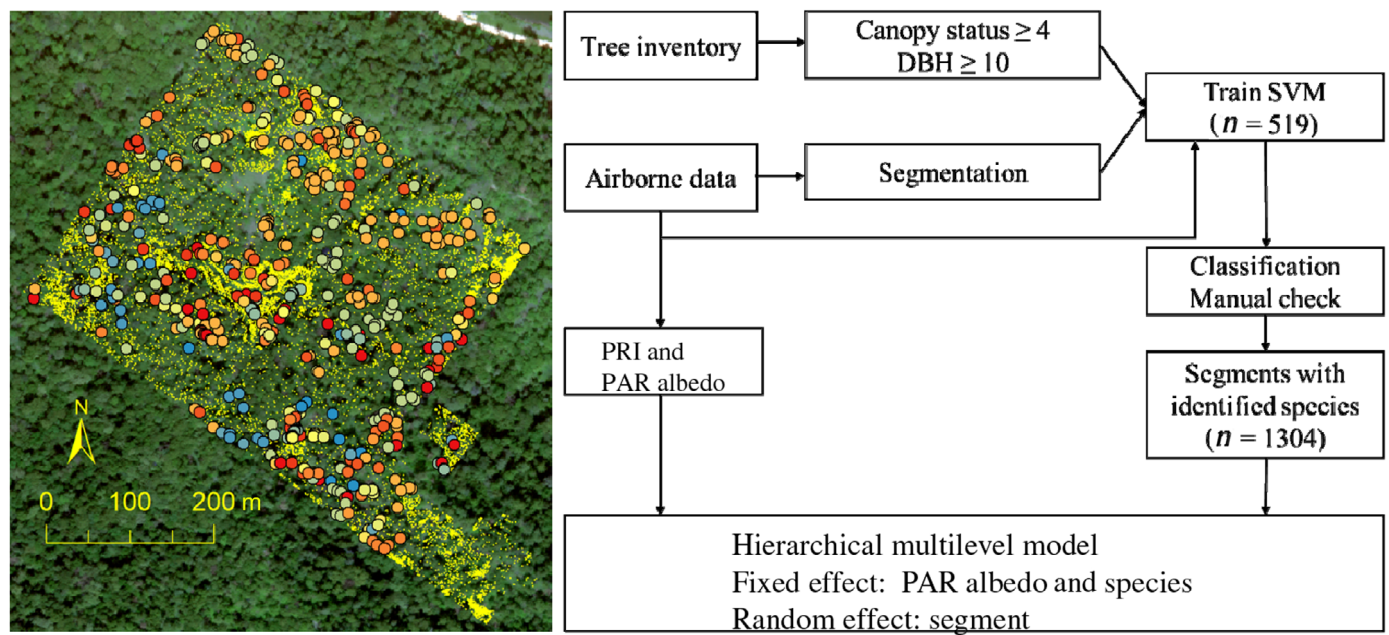


**Fig. 2** Locations of trees in the Indian Cave forest inventory plot (ICP) in a broad-leaved temperate forest in Nebraska, USA (left) and workflow for data collection and analysis (right). All trees in the ICP are mapped (small yellow dots) on top of true-color reflectance image derived from our data. Large dots, colored by species, indicate segments linked to 519 canopy trees used in the training dataset. DBH, trunk diameter at breast height;  $n$ , the number of segments; PAR, photosynthetically active radiation; PRI, Photochemical Reflectance Index; SVM, support vector machine classifier. For three small statured species, the DBH  $\geq 10$  cm criterion was not used. See the [Materials and Methods](#) section for details.

the training data. The predicted species identities were compared with species identities the forest inventory data by cross-referencing the image and ground-based coordinates for segments and trees, respectively, and only those that were correctly identified were used in the subsequent hierarchical analysis. By combining SVM results and manual verification, we identified 1326 segments belonging to 28 species. Third, to ensure adequate statistical power for analyses, we removed species with  $< 10$  segments and segments comprised of  $< 10$  pixels, leading to a dataset that contained 1304 segments and 20 species. In most cases, a segment corresponded to a single tree crown, which is the case for tall-statured species. In some cases, a single large overstory tree crown could be assigned to a few segments due to within-crown spectral heterogeneity. Three smaller statured species (*Asimina triloba*, *Rhus glabra*, *Cornus drummondii*) that never reach DBH  $> 10$  cm reproduce vegetatively and form nearly monospecific clumps of smaller stems in more open areas that have canopy exposure  $\geq 4$ . For these species, if one region was covered by only one species, and all individuals had canopy exposure  $\geq 4$ , then they were included in the analysis. In these cases, a segment did not correspond to a single tree crown.

### Hierarchical modeling of the PRI-irradiance relationship

In this nested (pixel-segment-species) approach, neither pixels nor segments can be treated as having independent residual error. To account for this inherent lack of independence, we applied a hierarchical model to analyze the relationship between PRI and PAR albedo. Our model produced individual and species-level parameters (the intercept and slope of the PRI–PAR albedo

relationship) that are canopy-level analogues to the leaf-level parameters PRI<sub>0</sub> and  $\Delta$ PRI developed from detailed physiological measurements of leaf reflectance (e.g. Gamon & Berry, 2012), as described above.

First, we calculated PRI as:

$$\text{PRI} = \frac{\rho_{531} - \rho_{570}}{\rho_{531} + \rho_{570}} \quad \text{Eqn 1}$$

where  $\rho_{531}$  and  $\rho_{570}$  are the surface reflectance at wavelengths of 531 and 570 nm (Gamon *et al.*, 1993; Peñuelas *et al.*, 1995).

Then, using the PAR albedo for each pixel (described above in [Irradiance estimation](#) in the Materials and Methods section) we fit a multilevel model to the PRI–PAR albedo relationship:

$$\begin{aligned} \text{PRI}_{ij} &= \beta_0 + \beta_1 \times \text{PAR albedo}_{ij} + \varepsilon_{ij} \\ \beta_0 &= \gamma_{00} + \gamma_{01} \times \text{Species}_{ij} + \mu_{0j} \\ \beta_1 &= \gamma_{10} + \gamma_{11} \times \text{Species}_{ij} + \mu_{1j} \\ (\mu_{0j}, \mu_{1j}) &\sim N\left(0, \begin{bmatrix} \tau_{00}^2 & \rho\tau_{00}\tau_{11} \\ \rho\tau_{00}\tau_{11} & \tau_{11}^2 \end{bmatrix}\right) \\ \varepsilon_{ij} &\sim N(0, \sigma^2) \end{aligned} \quad \text{Eqn 2}$$

where PRI<sub>ij</sub> indicates the PRI value of the  $i^{\text{th}}$  pixel in the  $j^{\text{th}}$  segment. This model assumed fixed effect variation ( $\gamma_{00}$ ,  $\gamma_{01}$ , and  $\gamma_{10}$ ,  $\gamma_{11}$ ) of the intercept ( $\beta_0$ ) and slope ( $\beta_1$ ) by species, as well as random effect variation ( $\mu_{0j}$  and  $\mu_{1j}$ ) of the intercept and slope among segments within species. We assumed that the PRI–PAR albedo relationship was linear among pixels within a segment,

**Table 1** Correspondence between model parameters (intercept and slope) of the relationship between the Photochemical Reflectance Index (PRI) and photosynthetically active radiation (PAR albedo) (first column), the interpretation of dark-state PRI ( $PRI_0$ ) and  $\Delta PRI$  (middle column), and their hypothesized physiological implications and ecophysiological interpretations (last column), involving photosynthetic stress responses related to constitutive responses associated with slowly changing pigment pools and facultative responses associated with more dynamic conversion of xanthophyll cycle pigments.

Parameter values of PRI–PAR albedo relationship	Model interpretation	Physiological interpretation and ecophysiological implications
Lower intercept	Lower PRI value at zero illumination (lower dark-adapted PRI, $PRI_0$ )	Lower chlorophyll : carotenoid pigment ratios indicative of greater investment in photoprotective pigments (and possibly more sustained non-photochemical quenching) due to chronic exposure to stressors that reduce photosynthetic light use efficiency (LUE)
Higher intercept	Higher PRI value at zero illumination (higher dark-adapted PRI, $PRI_0$ )	Higher chlorophyll : carotenoid pigment ratios indicative of less relative investment in photoprotective pigments (and possibly less sustained non-photochemical quenching) due to less chronic exposure to stressors that reduce photosynthetic LUE
Shallower slope (closer to zero)	Smaller decline in PRI with irradiance (lower $\Delta PRI$ )	Weaker xanthophyll cycle response, less reversible non-photochemical quenching, and less photosynthetic downregulation with increasing sunlight, indicative of mild photoprotective responses and maintenance of photosynthetic LUE with greater illumination
Steeper slope (more negative)	Large decline in PRI with irradiance (higher $\Delta PRI$ )	Stronger xanthophyll cycle response and more photosynthetic downregulation with increasing light, implying greater declines in photosynthetic LUE as more absorbed energy is diverted to reversible non-photochemical quenching via the xanthophyll cycle

which was confirmed by inspection of scatterplots for each segment. The multilevel model was implemented using the *lmer* function in the LME4 R package (Bates *et al.*, 2015). Fitted relationships with 95% confidence intervals, either including or excluding variation accounted for in the random effects model, were plotted using the GGEFFECTS R package (Lüdtke, 2018).

We used model selection based on Akaike information criterion (AIC) and likelihood ratio tests to evaluate four candidate models of varying complexity to test the hypothesis that accounting for illumination improved our ability to detect differences between species in their PRI responses. We used *pseudo- $R^2$*  statistics calculated using the MuMIn R package (Barton, 2009) to test whether greater variance in PRI was explained by accounting for variation among species in the PRI–PAR albedo relationship and to compare the amount of variation at the individual vs species levels. The marginal *pseudo- $R^2$*  ( $R^2_M$ ) represents the proportion of variance in the response variable explained by the fixed effect model alone, and the conditional *pseudo- $R^2$*  ( $R^2_C$ ) represents the proportion explained by both the fixed and random effects models (Nakagawa & Schielzeth, 2013). Diagnostics showed that residual errors met the assumptions of normality and homoscedasticity. We used *post hoc* pairwise comparisons to identify species that differed significantly in intercept and slope estimates, after controlling the false discovery rate (Benjamini & Hochberg, 1995). All statistical analyses were performed using the R statistical software (R Core Development Team, 2019).

### Physiological interpretation of model parameters

Our study assumed that the PRI responses of segments representing individual tree crowns represent aggregated leaf-level photosynthetic and photoprotective light responses that correspond to those described in the Introduction for individual leaves and

canopy regions (e.g. Gamon & Berry, 2012; Gamon & Bond, 2013). In our model, the intercept (PRI at PAR albedo = 0) provided a proxy for  $PRI_0$  (the dark-state PRI corresponding to the constitutive PRI response correlated with slowly changing pigment pool sizes), whereas the slope, which quantifies the change in PRI with PAR albedo, represented a proxy for  $\Delta PRI$  (the facultative response corresponding to changes in the xanthophyll cycle pigment response to irradiance). These parameters and their interpretation are summarized in Table 1. Differences in the intercept or slope between segments or species correspond to differences in slowly changing (constitutive) or rapidly changing (facultative) photoprotective responses, as indicated by the four different lines in Fig. 3, which represent hypothetical PRI–light responses of different segments (tree crowns). The responses of species and tree crowns can involve both, due to differences in the constitutive levels of photosynthetic pigments ( $PRI_0$ ) and in the capacity to engage dynamic photoprotective mechanisms of the xanthophyll cycle with changing irradiance ( $\Delta PRI$ ).

### Results

PAR albedo, the irradiance proxy, and PRI values exhibited coherent patterns associated with topography (Fig. 4a,b). Higher PAR albedo values (warmer colors in Fig. 4a) occurred near south and west-facing ridgetops (indicated by blue lines). By contrast, lower PAR albedo values were found in the valleys and north-east facing slopes (blue colors in Fig. 4a). The Photochemical Reflectance Index generally varied inversely with PAR albedo, with higher PRI values located towards the valley bottoms and on north-east facing slopes (warmer colors, Fig. 4b). PAR albedo and PRI of segments (tree crowns) were similarly structured by topography (Fig. 4c,d), demonstrating the importance of landscape and individual-level effects on photoprotective responses.

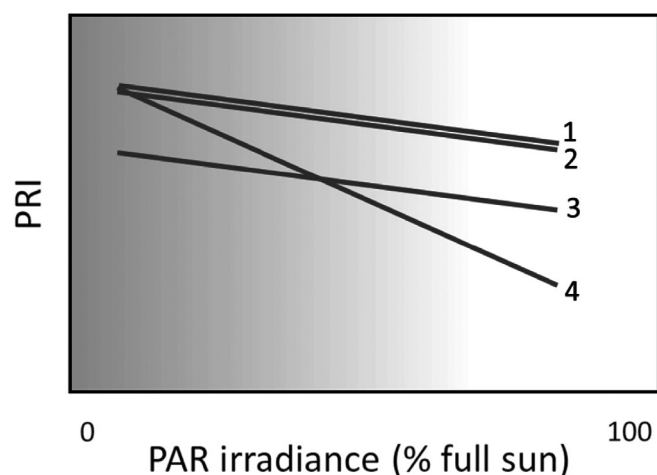


**Fig. 3** Hypothetical Photochemical Reflectance Index (PRI) responses to irradiance (photosynthetically active radiation (PAR) albedo). Lines 1–4 represent different segments (tree crowns), each of which is comprised of a number of pixels. The shading represents an illumination gradient, ranging from deep shade (0%) to full sun (100%). Segments can have similar (1, 2, 4) or different (1, 2, 4 vs 3) dark-state values (intercept,  $PRI_0$ ), and either similar (1, 2, 3) or different (1, 2, 3 vs 4) responses to irradiance (slope,  $\Delta PRI$ ). See Table 1 for further explanation of slopes and intercepts.

Segment-level PAR albedo was higher (warmer colors) for segments towards ridgetops, particularly on south and west-facing slopes, and declined towards the valley bottoms (cooler colors) (Fig. 4c). Segment-level PRI tended to follow an inverse pattern, with lower values concentrated on south and west-facing ridgetops (cooler colors), and higher values in the valley bottoms (warmer colors) (Fig. 4d).

Variation in PRI was primarily explained by PAR albedo, but species also differed in their PRI–PAR albedo responses. Among the four models tested, the model containing the fixed-effects interaction between species and PAR albedo was the most supported by the data ( $\chi^2 = 108.73$ ,  $P < 0.001$ ), and illustrated significant variation among species in their PRI–PAR albedo relationship, even after accounting for segment-level variation. Among the models tested, the best model provided a substantially better fit to the data than the model excluding PAR albedo in which species were allowed to differ only in PRI. Thus, adding PAR albedo and its interaction with species enhanced the model's ability to explain stand-level variation in PRI. Based on *pseudo-R*<sup>2</sup> statistics, both the fixed-effect (species-level) and the random-effect (segment-level) models explained substantial variation in PRI (Table 2). While the fixed-effect model alone explained a large amount of variation in PRI ( $R^2M$ ), indicating the importance of accounting for species' differences in the PRI–PAR albedo relationship (Table 3), the high values of  $R^2C$  indicate that there was also substantial individual-level variation in the PRI–PAR albedo relationship within species.

Across all pixels associated with tree crowns, the PRI exhibited a strong light response, as expected. Overall, this relationship appeared nonlinear. However, the PRI–PAR albedo relationship for each segment varied linearly in nearly all cases. Thus, the overall nonlinear PRI–PAR albedo relationship arose because of variation in the segment-specific intercepts and slopes of the relationship

with PAR albedo (Fig. 5). Segments with overall higher PAR albedo had lower intercepts (Fig. 5b) and shallower slopes (closer to zero; Fig. 5c) than segments with lower PAR albedo, indicating a correlation between the two PRI components.

Examination of the parameters of the PRI–PAR albedo relationship allowed us to explore the degree to which interspecific variation in PRI–light responses were likely driven by constitutive vs facultative effects (as in Fig. 3 and Table 1). Pairwise comparisons showed that in many cases, species did not differ significantly in slope or intercept ( $P > 0.05$ ; blue squares in Fig. 6). However, several pairs of species did differ in slopes, intercepts, or both (orange squares in Fig. 6), suggesting interspecific variation in photoprotection. For example, the intercept for bitternut hickory (*Carya cordiformis*) was significantly higher than several species, especially other canopy tree species of similar stature, such as several oaks (*Quercus* spp.), American ash (*Fraxinus americana*), and black walnut (*Juglans nigra*), but also some smaller-statured species, including dogwood (*Cornus drummondii*) (Figs 6, 7a; Table 3). This indicates that compared with many species, bitternut hickory had higher chlorophyll : carotenoid pigment ratios, suggesting that its photosynthetic strategy is characterized by less constitutive investment in photoprotective pigments. By contrast, a greater number of pairs of species differed significantly in their slopes, and this was especially true of the oaks (*Quercus* spp.) and American basswood (*T. americana*). For example, the slope for American basswood was significantly steeper than that of all oaks (Figs 6, 7a; Table 3), suggesting that basswood had a stronger xanthophyll cycle pigment response and steeper declines in photosynthetic LUE with increasing light. Together, the PRI–PAR albedo responses suggest species' differences in pigment pool sizes and xanthophyll cycle responses, represented by the intercept and slope of the PRI–PAR albedo relationship, respectively.

The importance of accounting for both species and individual-level variation in the PRI–PAR albedo relationship is illustrated through closer examination of three species: bitternut hickory (*Carya cordiformis*), Northern red oak (*Quercus rubra*), and American basswood (*Tilia Americana*) (Fig. 6). These species differ significantly in their PRI–PAR albedo relationships, after accounting for individual-level variation (Fig. 7a; Table 3). However, individual-level variation is still quite important in interpreting the PRI–PAR albedo relationship for each species (Fig. 6b–d). Individuals of a species not only have different average illumination (variation in the position of the black lines on the *x*-axis) and PRI (variation in the positions of the black lines on the *y*-axis), but also have different PRI–albedo relationships (variation in slopes and intercepts between lines). The variation in PRI–PAR albedo relationships among segments within species suggests substantial intraspecific (individual-level) variation in photoprotective responses in this topographically heterogeneous landscape.

## Discussion

Proximal measurements have established that the PRI–light relationship provides a measure of constitutive pigment levels



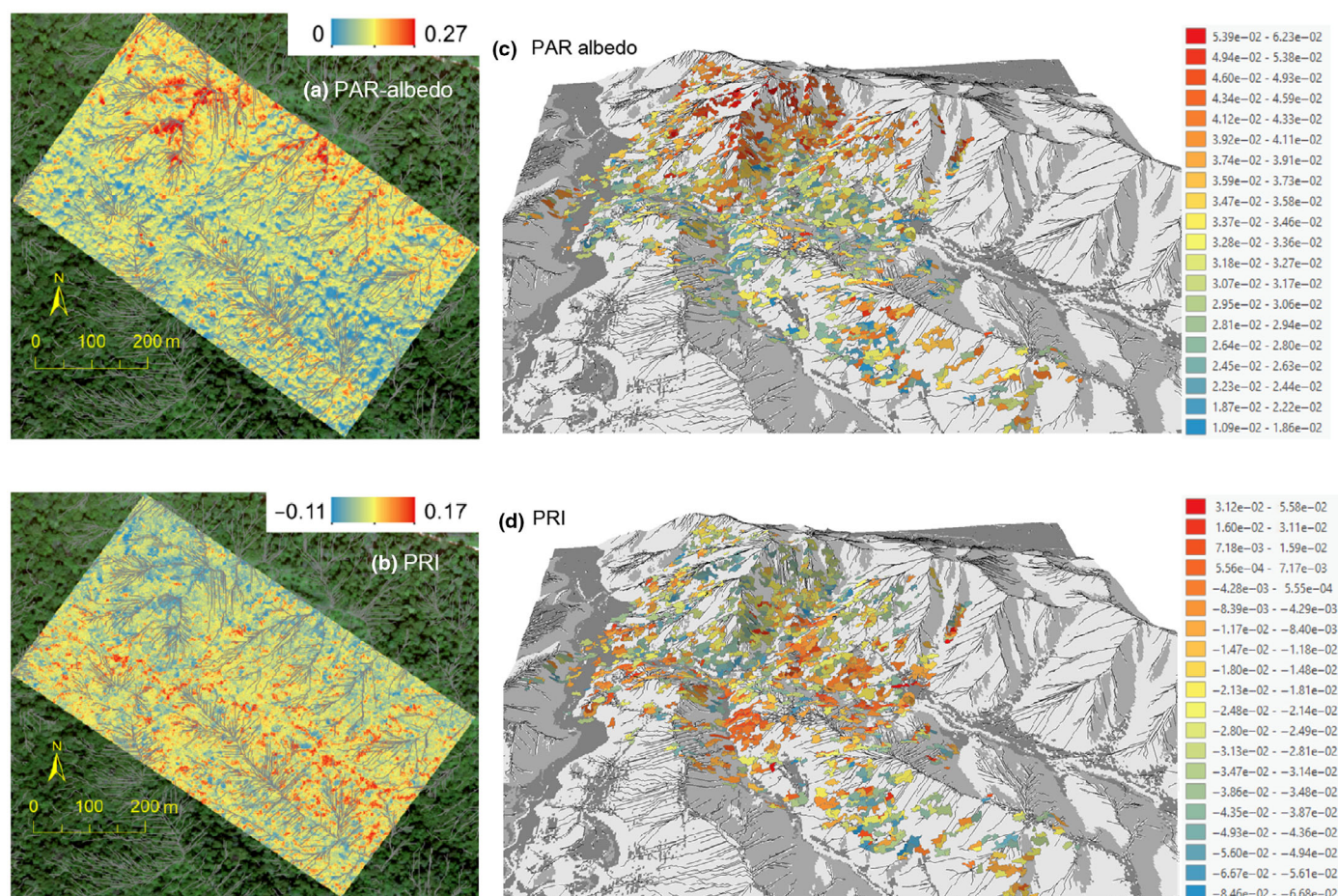


**Fig. 4** Landscape variation in photosynthetically active radiation (PAR) albedo and the Photochemical Reflectance Index (PRI) in the Indian Cave forest inventory plot (ICP) in a broad-leaved temperate forest in Nebraska, USA. Pixel-level variation in PAR albedo (a) and PRI (b) values overlaid on a true-color reflectance image of the ICP and surrounding forest. Higher values are shown in red, and lower values are shown in blue. Segment-level variation in PAR albedo (c) and PRI (d) values in the ICP. Average PAR albedo and PRI for segments, which correspond to individual tree crowns, are plotted on a color ramp (higher values in red and lower values in blue) and overlaid on a 3-dimensional topographic rendition for the portion of the Indian Cave plot in which trees have been georeferenced and identified to species. Ridgelines are indicated with gray lines. In (c) and (d), hill-shading indicates variation in aspect (darker shading corresponds to northeastern aspects and lighter shading to southwestern aspects).

and the dynamic engagement of photoprotection via the xanthophyll cycle in response to changes in illumination, making the light response fundamental to interpreting this index. Here, we demonstrate that variation in the PRI-light relationship can be quantified using airborne imaging spectroscopy to reveal variation in photoprotection among individual tree crowns and species, even in complex forested landscapes. At the individual level, this variation was often correlated with topographic position, suggesting that trees and species in this forest have different photoprotective strategies depending on exposure and access to soil moisture, which affect desiccation stress and photosynthetic activity.

Our study presents a new way to quantify functional diversity through photoprotective responses using airborne imaging spectrometry and a hierarchical statistical framework applied to the light response of PRI. This method allows us to evaluate photoprotective behavior of individual canopy trees and tree species, revealed as slopes and intercepts in a multilevel model describing PRI-light responses at multiple scales. These model parameters

have analogues to those previously developed at leaf and canopy scales, as described in the [Introduction](#). Our findings are uniquely possible with airborne imaging spectrometry, which can provide the hyperspectral resolution needed for quantifying PRI, the spatial resolution to distinguish the responses of individual tree crowns and species, and sufficient spatial extent to sample entire forest stands.

Unlike most satellite remote sensing with coarse pixels, fine-scale airborne imaging spectrometry allows the detection, visualization, and quantitative analysis of photoprotective PRI responses of individual tree crowns and species located in structurally complex forests. With this fine pixel resolution, the effects of differential illumination on PRI variation can be characterized in a single overpass, thereby constraining several factors that confound PRI interpretation in most remote sensing campaigns, and allowing us to detect diversity in individual and species-level photoprotective responses. Such inferences are generally not available with satellite sensors operating at coarser scales, nor are they easily obtainable from field surveys that have difficulty accessing the

**Table 2** Model comparison and test statistics for four nested hierarchical models relating the Photochemical Reflectance Index (PRI) to photosynthetically active radiation (PAR albedo) and species identity.

Model and factors	F-value	P
Full Model (AIC = −475430.6; logLik = 237759.3; $R^2M$ = 0.545; $R^2C$ = 0.840)		
PAR albedo	1591.014	< 0.001
Species	5.358	< 0.001
PAR albedo × Species	7.333	< 0.001
PAR albedo + Species Model (AIC = −475359.9; logLik = 237704.9; $R^2M$ = 0.544; $R^2C$ = 0.845)		
PAR albedo	5923.592	< 0.001
Species	18.101	< 0.001
PAR albedo Model (AIC = −467269.8; logLik = 233638.9; $R^2M$ = 0.550; $R^2C$ = 0.790)		
PAR albedo	58 720	< 0.001
Species Model (AIC = −423719.8; logLik = 211881.9; $R^2M$ = 0.130; $R^2C$ = 0.560)		
Species	19.573	< 0.001

Model selection was performed for the fixed effect models shown in the table, and all random effects model included segment-level variation. The marginal pseudo- $R^2$  ( $R^2M$ ) represents the proportion of the variance in PRI explained by the fixed effects model alone, and the conditional pseudo- $R^2$  ( $R^2C$ ) explains the proportion explained by the fixed and random models together.

top of the forest canopy. The evaluation of PRI-light responses from airborne imaging spectrometry offers a unique view of functional diversity with respect to photoprotection and photosynthetic downregulation of individual crowns, possibly providing early detection of differential exposure or vulnerability of tree species to environmental stressors.

### Light-dependent variation in PRI at multiple scales

Our study revealed clear landscape patterns both in crown illumination (estimated as PAR albedo) and foliar photoprotective responses (measured using PRI). More sunlit regions (hilltops and south-facing slopes) exhibited higher PAR albedo and lower PRI values (Fig. 4), suggesting greater photosynthetic downregulation and photoprotection of individual trees in these regions. Trees in these locations typically face more sun exposure, evaporative demand, and drier soils than in the valley bottoms, which exhibited higher PRI values. These results indicate that variation in the PRI-light response provides useful information on photoprotective behaviour related to the irradiance patterns experienced by individual tree crowns in topographically complex landscapes.

The strong negative relationship between PRI and PAR albedo is consistent with a large body of experimental studies employing proximal spectral reflectance at the leaf and canopy scales showing that PRI responds to illumination (Gamon *et al.*, 1990, 1992; Gamon & Surfus, 1999; Gamon & Berry, 2012; Hmi-mina *et al.*, 2014). Similar responses have been observed in intact forest stands using a spectrometer mounted on a pan and tilt platform attached to a tower (e.g. Hall *et al.*, 2008; Hilker *et al.*, 2008). PRI-light responses have also been explored from satellite using multi-angle MODIS sensor samples at 1-km

**Table 3** Intercept and slope parameter estimates and standard errors (SE) for the Photochemical Reflectance Index (PRI)–photosynthetically active radiation (PAR) albedo relationship for 20 woody species in a temperate broad-leaved forest in Nebraska, USA.

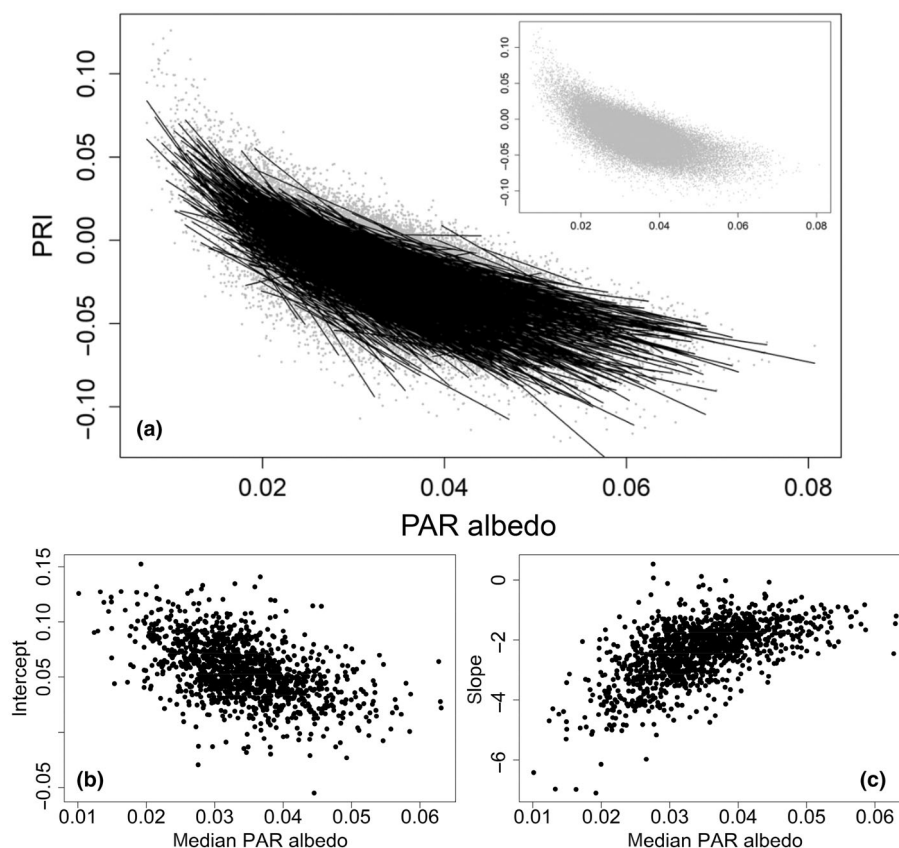
Species code	Scientific name (family)	PRI–PAR albedo relationship			
		Intercept	Intercept SE	Slope	Slope SE
ASIMTR	<i>Asimina triloba</i> (L.) Dunal (Annonaceae)	0.0628	0.0043	−2.785	0.147
CARYCO	<b><i>Carya cordiformis</i></b> (Wangenh.) K. Koch (Juglandaceae)	<b>0.0761</b>	<b>0.0049</b>	<b>−3.055</b>	<b>0.166</b>
CARYOV	<i>Carya ovata</i> (Mill.) K. Koch (Juglandaceae)	0.0641	0.0063	−2.678	0.208
CELTOC	<i>Celtis occidentalis</i> L. (Cannabaceae)	0.0583	0.0054	−2.742	0.180
CORNDR	<i>Cornus drummondii</i> C.A. Mey. (Cornaceae)	0.0156	0.0153	−1.518	0.506
FRAXAM	<i>Fraxinus americana</i> L. (Oleaceae)	0.0540	0.0038	−2.225	0.126
GYMNDI	<i>Gymnocladus dioica</i> (L.) K. Koch. (Fabaceae)	0.0668	0.0116	−2.727	0.390
JUGLNI	<i>Juglans nigra</i> L. (Juglandaceae)	0.0563	0.0032	−2.693	0.106
MORURU	<i>Morus rubra</i> L. (Moraceae)	0.0692	0.0077	−2.827	0.258
OSTRVI	<i>Ostrya virginiana</i> (Mill.) K. Koch (Betulaceae)	0.0412	0.0141	−2.261	0.454
PLATOC	<i>Platanus occidentalis</i> L. (Platanaceae)	0.0628	0.0087	−2.809	0.295
QUERMA	<i>Quercus macrocarpa</i> Michx. (Fagaceae)	0.0481	0.0033	−2.227	0.111
QUERMU	<i>Quercus muehlenbergii</i> Engelm. (Fagaceae)	0.0460	0.0018	−2.034	0.059
QUERRU	<b><i>Quercus rubra</i> L.</b> (Fagaceae)	<b>0.0647</b>	<b>0.0019</b>	<b>−2.438</b>	<b>0.065</b>
QUERVE	<i>Quercus velutina</i> Lam. (Fagaceae)	0.0486	0.0041	−1.948	0.137
RHUSGL	<i>Rhus glabra</i> L. (Anacardiaceae)	0.0597	0.0046	−2.226	0.150
TILIAM	<b><i>Tilia americana</i> L.</b> (Malvaceae)	<b>0.0638</b>	<b>0.0036</b>	<b>−3.108</b>	<b>0.120</b>
ULMUAM	<i>Ulmus americana</i> L. (Ulmaceae)	0.0643	0.0084	−2.821	0.285
ULMURU	<i>Ulmus rubra</i> Muhl. (Ulmaceae)	0.0524	0.0072	−2.685	0.243
ULMUTH	<i>Ulmus thomasi</i> Sarg. (Ulmaceae)	0.0292	0.0190	−1.521	0.628

Estimates were derived from the most-supported model, which included the species × PAR albedo interaction (Table 2). Rows in boldface are the species shown in Fig. 7.

resolution (Drolet *et al.*, 2008; Middleton *et al.*, 2016). However, at that spatial scale, effects of landscape heterogeneity, species, individuals, and canopy illumination patterns cannot be resolved,



**Fig. 5** Variation in the Photochemical Reflectance Index (PRI) response to photosynthetically active radiation (PAR) albedo in the Indian Cave forest inventory plot (ICP) in a broad-leaved temperate forest in Nebraska, USA. In (a) dots represent individual pixels associated with all 1304 of the analyzed segments, and the black lines are best-fit lines corresponding to these segments based on the parameter estimates from the multilevel model. In the inset, individual points are plotted without the fitted lines for each segment to better show the observed relationship for all pixels. Panels (b, c) show variation in the segment-level intercept (b) and slope (c) of the PRI–PAR albedo relationship with respect to the segment's median PAR albedo.



as they are combined in a single sample, which confounds the interpretation of PRI. Moreover, the different MODIS PRI formulation and difficulties with validation over large spatial scales add to this uncertainty, leaving unclear the exact mechanism and interpretation of the PRI response in coarse satellite imagery. A possible alternative would be to use diurnal imagery to assemble a PRI–light response, but such data are not available from satellites with single overpass times and rarely obtained from aircraft due to the high costs of flights and complications of diurnally changing sky conditions (e.g. afternoon clouds, which are common in many areas of the world). Diurnal remotely sensed data can be further confounded by the interaction of physiological and structural responses due to changing sun angle, view angle, and sky conditions, presenting additional challenges in interpreting PRI–light responses (Suarez *et al.*, 2008; Biriukova *et al.*, 2020). By accounting for illumination and sampling at the subcanopy level in a single, rapid overpass with a constrained sampling geometry, our airborne method reduces several of these complications and provides coherent light responses that reveal contrasting photoprotection associated with different species and landscape positions.

By developing a proxy for illumination and incorporating it into a multilevel model of the PRI–light response at subcrown scales, our study provides a quantitative framework for investigating mechanistic variation in photoprotective and photosynthetic responses in complex forested landscapes. This framework not only enables more detailed analysis at multiple scales than possible with previous stand-level methods but also considers both

facultative and constitutive components of the PRI–light response, which, to our knowledge, have not previously been characterized using airborne imaging spectroscopy. These responses are analogous to the rapidly reversible and sustained responses of photoprotective xanthophyll cycle pigments (Demmig-Adams & Adams, 2006; Verhoeven, 2014; Walter-McNeill *et al.*, 2021), often expressed as reversible and sustained NPQ, and likely represent distinct photoprotective mechanisms operating over different timescales.

### Quantifying contrasting photoprotective responses

Interspecific variation in species' photosynthetic and photoprotective responses have been demonstrated in a tropical forest stand using optical measurements from a canopy access crane (Gamon *et al.*, 2005), experimental prairie plots (Kothari *et al.*, 2018), and in common garden studies (Gamon *et al.*, 1997; Walter-McNeill *et al.*, 2021). Consistent with these proximal studies, our multilevel model also showed that tree species in this Nebraskan forest can differ in photoprotective responses. Interspecific comparisons of the intercepts (corresponding to  $PRI_0$ ) and slopes (corresponding to  $\Delta PRI$ ) of the PRI–PAR albedo relationship (Fig. 6) suggest that species' differences in PRI values at this forest site result from both constitutive effects (pool sizes of pigments involved in photosynthesis and sustained photoprotection) and facultative responses (readily reversible xanthophyll cycle effects). Pigment pool sizes are known to vary more slowly than the xanthophyll cycle response and may



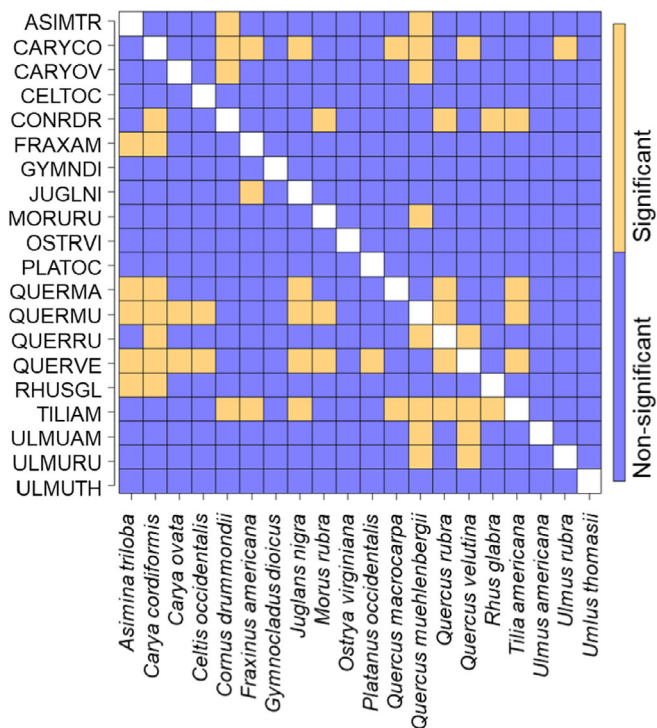


**Fig. 6** Pairwise differences between tree species in slope (bottom left triangle) and intercept (top right triangle) parameter estimates of the Photochemical Reflectance Index (PRI)-photosynthetically active radiation (PAR) albedo relationship in the Indian Cave forest inventory plot, NE, USA. Pairs of species that were statistically significant ( $\delta = 0.05$ ) after controlling for the false discovery rate are shown in orange, whereas non-significant pairs are shown in blue.

reflect species' long-term investment in photoprotective pigments, as well as the integrated light environment and stressors over ontogenetic (Gamon & Surfus, 1999; Gamon & Berry, 2012) and seasonal (Wong & Gamon, 2015; Wong *et al.*, 2019) time frames. By contrast, the short-term xanthophyll cycle effect responds rapidly to diurnal changes in illumination when temperatures are warm enough to support active biochemistry, offering a readily reversible photoprotective mechanism (Demmig-Adams & Adams, 1996). By considering both mechanisms together, PRI-light responses allow a comprehensive view of photoprotection that has been hard to achieve with previous remote sensing studies unable to fully characterize the variation of PRI with illumination at the crown scale. Explicit consideration of PRI responses in the context of illumination, species identity, and landscape position improves the power of this index and advances our understanding of its spatial and temporal dynamics, thereby improving the physiological and ecological interpretation of photoprotection.

While many species differed in the intercepts and slopes of the PRI-PAR albedo relationship (Fig. 6), there were also substantial differences among individuals of the same species, as demonstrated by the considerable variation in PRI explained by the random effect terms of our hierarchical model. This within-species variation likely reflects the particular environmental conditions associated with an individual's location, and possibly genotypic variation between individuals within a species. Compared with

trees having higher average PAR albedo, trees with lower average estimated illumination often had higher intercepts (Fig. 5), indicating less standing investment in photoprotective carotenoid pigments and possibly less sustained photoprotection. These trees also tended to have steeper slopes in the PRI-PAR albedo relationship, suggesting a stronger xanthophyll cycle response. These patterns indicate that photoprotective responses are often correlated and can function in complementary ways.

Compared with the PRI response, many plant traits detectable by remote sensing, such as leaf mass per area (LMA), are considered relatively static; while they exhibit substantial variation within and between individuals and species (e.g. Bin *et al.*, 2022), they have not been found to exhibit rapid temporal changes. However, photosynthetic and photoprotective traits are very dynamic in both time and space and are easily disturbed by many proximal sampling methods. Some of these methods involve collecting leaf samples (often difficult to obtain from tree-tops) and transporting them back to the laboratory for later analysis, which alters the light environment, temperature, hydration, and other factors influencing photosynthesis. Our understanding of such dynamic plant characteristics can benefit from further development of rapid and spatially extensive *in situ* methods that offer minimal disturbance, a strength of airborne imaging spectroscopy as demonstrated in this study.

In the months before our 2019 airborne campaign, the study region received record precipitation combined with rapid spring warming that led to extensive flooding along the Missouri River that persisted into fall (Flanagan *et al.*, 2020). As a result, the valleys and lower elevation soils of our study site remained consistently moist at the time of the overflight. However, the soils on the ridgetops and higher elevations were far drier, as they are well-drained soils derived from loess (Elder, 1969; Joekel *et al.*, 2019; Soil Survey Staff, 2021). These conditions likely influenced the topographically driven PRI-PAR albedo responses reported here (Fig. 4). These patterns are also expected to vary with season and time of day, illustrating the value of imaging spectroscopy to characterize shorter term physiological responses to environmental conditions, particularly as temperature and hydrological conditions change, and climate extremes become more frequent (AghaKouchak *et al.*, 2020).

These airborne methods of sampling dynamic physiological responses may be of use not only in functional studies addressing ecological questions but would also benefit other fields of plant science where evaluating spatial or temporal patterns in species photosynthetic and stress responses is important. PRI has emerged as a previsual detector of stress in precision agriculture (Wong *et al.*, 2022), phenotyping (Machwitz *et al.*, 2021), and disease detection (Zarco-Tejada *et al.*, 2021). The PRI-PAR albedo relationship derived from imaging spectroscopy, combined with the analytical framework developed here that allows for improved physiological interpretation, may be a useful early warning indicator of stress responses, particularly when combined with other metrics. Potential applications of this approach include ecology, plant physiology, phenotyping, precision agriculture, and forestry, all of which benefit from rapid, extensive methods for assessing photosynthetic stress responses of

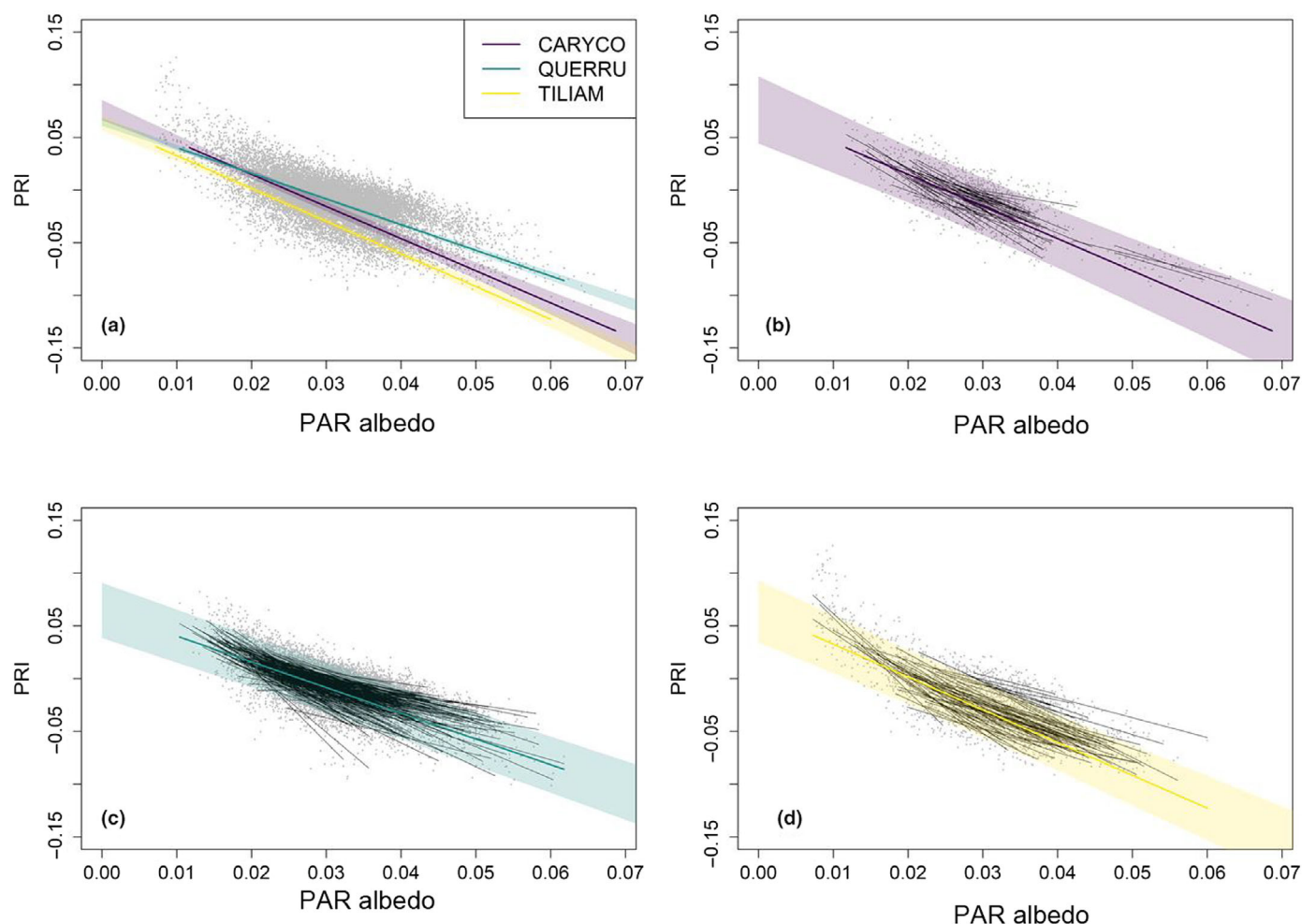


**Fig. 7** Variation in the Photochemical Reflectance Index (PRI) response to photosynthetically active radiation (PAR) albedo for three tree species in the Indian Cave forest inventory plot (ICP) in a broad-leaved temperate forest in Nebraska, USA. In (a), the best-fit lines for each species are shown, with 95% confidence ribbons based on the fixed effects only (i.e. excluding segment-level variation within species). Species are *Carya cordiformis* (CARYCO), *Quercus rubra* (QUERRU), and *Tilia americana* (TILIAM). Gray dots represent individual pixels corresponding to these species. Panels (b–d) show separate plots for the same three species with black lines corresponding to the fits for each individual (segment). In contrast to (a), 95% confidence ribbons were estimated including individual-level variation accounted for in the random-effects model and hence are wider than in (a). See Table 3 for intercept and slope estimates by species.

individuals, genotypes, and species in settings ranging from monocultures to complex landscapes.

### Conclusions and recommendations for future work

In this study, we present a hierarchical framework for distinguishing individual tree crown and species photoprotective responses to irradiance detected using airborne imaging spectrometry. Using extensive ground sampling, we were able to validate species identities for 1304 individual tree crowns and thus demonstrate substantial variation in photoprotective responses within and between species. We acknowledge that some of our interpretations of the PRI-light response have not been fully validated at this scale, and so we present them as hypotheses to be tested in future studies. However, our interpretations rest on a rich history of proximal research linking PRI-light response to photoprotection through independent physiological measurements. The large

sample sizes obtained in a few seconds from a single airborne overpass simply cannot be simultaneously sampled from the ground using conventional physiological methods (e.g. gas exchange or pigment assays) which typically require many minutes for a single leaf sample and are even more complicated to conduct in the field on top-canopy leaves. Potential approaches to validation could involve independent sampling of canopy structure, incident irradiance, and contrasting physiological responses via surface temperature, leaf-level optical and pigment samples, chlorophyll fluorescence, and gas exchange, some of which can be assisted with canopy access drones (Charron *et al.*, 2020), and all of which were clearly beyond the scope of this study. Alternative approaches to evaluate these results could include canopy radiative transfer modeling linked to photosynthesis models (e.g. Yang *et al.*, 2021). Such integrated modeling approaches are relatively new, would require detailed parameterizations of three-dimensional canopy structure, irradiance, leaf

physiology, and biochemistry, and have not yet fully incorporated PRI-light responses, and so remain a future goal.

Understanding the multiple factors influencing the responses of vegetation to stressors requires an integrative approach (Munson *et al.*, 2021), which could benefit from PRI as an early, previal stress indicator, particularly when combined with contextual information such as irradiance and species identity, all of which can be addressed with imaging spectrometry. Future work should explore possible links between these early physiological responses, model parameters describing the PRI–PAR albedo response, and longer term stand demographic dynamics for this and other forests. The Indian Cave plot is part of the ForestGEO global network of forest plots (Davies *et al.*, 2021), which offer opportunities for developing new capabilities for the remote sensing of forest diversity and function and could be instrumental in contributing to a global biodiversity monitoring system incorporating remote sensing (Jetz *et al.*, 2016; Wang & Gamon, 2019; Cavender-Bares *et al.*, 2020). Validation, tests of generality, and expansion of our approach will hopefully lead to an improved understanding of the relationships between short-term physiological responses and long-term stand dynamics and provide a unified framework for quantifying the resilience of forests to environmental change across spatial scales and forested biomes.

## Acknowledgements

We acknowledge the US Department of Agriculture Service Center Agencies for use of Digital Elevation Models from the USGS National Map 3DEP Downloadable Data Collection. Funding for flight support was provided by the University of Nebraska–Lincoln, and by the ‘PhotoProxy’ (for FLEX Campaign) contract to JAG from the European Space Agency (ESA) via Forschungszentrum Jülich (ESA Contract no. 4000125731/19/NL/LF) and NSF/NASA Dimensions of Biodiversity funding (DEB-1342823) to JAG. We thank the University of Nebraska–Lincoln and Jacqueline B. Mars for financial support of the Indian Cave forest inventory plot. Funding to complete this study was provided by a United States Department of Agriculture USFS McIntire–Stennis award no. 7002574 to JAG, SER, and RW and a National Science Foundation AccelNet award (OISE 2020424) to SER. We thank the Nebraska Game and Parks Commission for permission to install and maintain the Indian Cave plot in Indian Cave State Park. We thank Krista Lang and Gerry Steinauer for support and assistance maintaining the Indian Cave plot.

## Competing interests

None declared.

## Author contributions

JAG conceived of the PRI-light response approach, SER conceived of the hierarchical model, and all authors developed the physiological interpretation of model parameters. RW conducted image processing and statistical analyses in consultation with

SER and JAG. SER supervised the installation and data collection in the Indian Cave forest inventory plot. All authors contributed equally to the study design, interpretation of results, and writing of the manuscript.

## ORCID

John A. Gamon  <https://orcid.org/0000-0002-8269-7723>  
Sabrina E. Russo  <https://orcid.org/0000-0002-6788-2410>  
Ran Wang  <https://orcid.org/0000-0002-3810-9103>

## Data availability

The airborne image data are available through NASA Land Processes Distributed Active Archive Center (LP DAAC) at <https://lpdaac.usgs.gov/products/aeahypicne1mv001/>. The Indian Cave ForestGEO plot data are archived at <https://forestgeo.si.edu/explore-data>.

## References

- AghaKouchak A, Chiang F, Huning LS, Love CA, Mallakpour I, Mazdiyasn I, Moftakhari H, Papalexio SM, Ragno E, Sadegh M. 2020. Climate extremes and compound hazards in a warming world. *Annual Review of Earth and Planetary Sciences* 48: 519–548.
- Alonso L, Van Wittenbergh S, Amorós-López J, Vila-Francés J, Gómez-Chova L, Moreno J. 2017. Diurnal cycle relationships between passive fluorescence, PRI and NPQ of vegetation in a controlled stress experiment. *Remote Sensing* 9: 770.
- Asner GP, Nepstad D, Cardinot G, Ray D. 2004. Drought stress and carbon uptake in an Amazon forest measured with spaceborne imaging spectroscopy. *Proceedings of the National Academy of Sciences, USA* 101: 6039–6044.
- Atherton J, Olascoaga B, Alonso L, Porcar-Castell A. 2017. Spatial variation of leaf optical properties in a boreal forest is influenced by species and light environment. *Frontiers in Plant Science* 8: 309.
- Barton CVM, North PRJ. 2001. Remote sensing of canopy light use efficiency using the Photochemical Reflectance Index: model and sensitivity analysis. *Remote Sensing of Environment* 78: 264–273.
- Barton K. 2009. *MuMIn: multi-model inference*. R package v.0.12.0. [WWW document] URL <https://r-forge.r-project.org/projects/mumin/> [accessed 23 April 2021].
- Bates D, Mächler M, Bolker BM, Walker SC. 2015. Fitting linear mixed-effects models using lme4. *Journal of Statistical Software* 67: 1–48.
- Benjamini Y, Hochberg Y. 1995. Controlling the false discovery rate: a practical and powerful approach to multiple testing. *Journal of the Royal Statistical Society. Series B (Methodological)* 57: 289–300.
- Berk A, Anderson GP, Acharya PK, Shettle EP. 2008. *MODTRAN® 5.2.0.0 User's Manual*. Burlington MA and Hanscom MA, USA: Spectral Sciences Inc. and Air Force Research Laboratory.
- Bin Y, Li Y, Russo SE, Cao H, Ni Y, Ye W, Lian J. 2022. Leaf trait expression varies with tree size and ecological strategy in a subtropical forest. *Functional Ecology* 36: 1010–1022.
- Biriukova K, Celesti M, Evdokimov A, Pacheco-Labrador J, Julitta T, Migliavacca M, Giardino C, Miglietta F, Colombo R, Panigada C *et al.* 2020. Effects of varying solar-view geometry and canopy structure on solar-induced chlorophyll fluorescence and PRI. *International Journal of Applied Earth Observation and Geoinformation* 89: 102069.
- Cavender-Bares J, Gamon JA, Townsend PA. 2020. *Remote sensing of plant biodiversity*. Cham, Switzerland: Springer Nature.
- Charron G, Robichaud-Courteau T, La Vigne H, Weintraub S, Hill A, Justice D, Bélanger N, Lussier DA. 2020. The DeLeaves: a UAV device for efficient tree canopy sampling. *Journal of Unmanned Vehicle Systems* 8: 245–264.



- Clark DA, Clark DB. 1992. Life history diversity of canopy and emergent trees in a neotropical rain forest. *Ecological Monographs* 62: 315–344.
- Condit R. 1998. *Tropical forest census plots: methods and results from Barro Colorado Island, Panama and a comparison with other plots*. Berlin, Germany: Springer.
- Damm A, Cogliati S, Colombo R, Fritsche L, Genangeli A, Genesio L, Hanus J, Peressotti A, Rademski P, Rascher U *et al.* 2022. Response times of remote sensing measured sun-induced chlorophyll fluorescence, surface temperature and vegetation indices to evolving soil water limitation in a crop canopy. *Remote Sensing of Environment* 273: 112957.
- Davies SJ, Abiem I, Abu Salim K, Aguilar S, Allen D, Alonso A, Anderson-Teixeira K, Andrade A, Arellano G, Ashton PS *et al.* 2021. ForestGEO: understanding forest diversity and dynamics through a global observatory network. *Biological Conservation* 253: 108907.
- Demmig-Adams B, Adams WW. 1996. The role of xanthophyll cycle carotenoids in the protection of photosynthesis. *Trends in Plant Science* 1: 21–26.
- Demmig-Adams B, Adams WW. 2000. Photosynthesis: harvesting sunlight safely. *Nature* 403: 371–374.
- Demmig-Adams B, Adams WW. 2006. Photoprotection in an ecological context: the remarkable complexity of thermal energy dissipation. *New Phytologist* 172: 11–21.
- Drolet GG, Middleton EM, Huemmrich KF, Hall FG, Amiro BD, Barr AG, Black TA, McCaughey JH, Margolis HA. 2008. Regional mapping of gross light-use efficiency using MODIS spectral indices. *Remote Sensing of Environment* 112: 3064–3078.
- Elder JA. 1969. *Soils of Nebraska*. Lincoln, NE: Conservation and Survey Division, University of Nebraska.
- Feng W, Qi S, Heng Y, Zhou Y, Wu Y, Liu W, He L, Li X. 2017. Canopy vegetation indices from *in situ* hyperspectral data to assess plant water status of winter wheat under powdery mildew stress. *Frontiers in Plant Science* 8: 1219.
- Filella I, Porcar-Castell A, Munné-Bosch S, Bäck J, Garbalsky MF, Peñuelas J. 2009. PRI assessment of long-term changes in carotenoids/chlorophyll ratio and short-term changes in de-epoxidation state of the xanthophyll cycle. *International Journal of Remote Sensing* 30: 4443–4455.
- Fischbein SA, Joeckel RM, Fielding CR. 2009. Fluvial-estuarine reinterpretation of large, isolated sandstone bodies in epicontinental cyclothem, Upper Pennsylvanian, northern Midcontinent, USA, and their significance for understanding late Paleozoic sea-level fluctuations. *Sedimentary Geology* 216: 15–28.
- Flanagan PX, Mahmood R, Umphlett NA, Haacker E, Ray C, Sorensen W, Shulski M, Stiles CJ, Pearson D, Fajman P. 2020. A hydrometeorological assessment of the historic 2019 flood of Nebraska, Iowa, and South Dakota. *Bulletin of the American Meteorological Society* 101: E817–E829.
- Fuentes DA, Gamon JA, Qiu H-I, Sims DA, Roberts DA. 2001. Mapping Canadian boreal forest vegetation using pigment and water absorption features derived from the AVIRIS sensor. *Journal of Geophysical Research: Atmospheres* 106(D24): 33565–33577.
- Gamon JA. 2015. Reviews and syntheses: optical sampling of the flux tower footprint. *Biogeosciences* 12: 4509–4523.
- Gamon JA, Berry JA. 2012. Facultative and constitutive pigment effects on the Photochemical Reflectance Index (PRI) in sun and shade conifer needles. *Israel Journal of Plant Sciences* 60: 85–95.
- Gamon JA, Bond B. 2013. Effects of irradiance and photosynthetic downregulation on the Photochemical Reflectance Index in Douglas-fir and ponderosa pine. *Remote Sensing of Environment* 135: 141–149.
- Gamon JA, Field CB, Bilger W, Björkman O, Fredeen AL, Peñuelas J. 1990. Remote sensing of the xanthophyll cycle and chlorophyll fluorescence in sunflower leaves and canopies. *Oecologia* 85: 1–7.
- Gamon JA, Filella I, Peñuelas J. 1993. The dynamic 531-nanometer  $\Delta$  reflectance signal: a survey of twenty angiosperm species. In: Yamamoto HY, Smith CM, eds. *Photosynthetic responses to the environment*. Rockville, MD, USA: American Society of Plant Physiologists, 172–177.
- Gamon JA, Kitajima K, Mulkey SS, Serrano L, Wright SJ. 2005. Diverse optical and photosynthetic properties in a neotropical dry forest during the dry season: implications for remote estimation of photosynthesis. *Biotropica* 37: 547–560.
- Gamon JA, Kovalchuk O, Wong CYS, Harris A, Garrity SR. 2015. Monitoring seasonal and diurnal changes in photosynthetic pigments with automated PRI and NDVI sensors. *Biogeosciences* 12: 4149–4159.
- Gamon JA, Peñuelas J, Field CB. 1992. A narrow-waveband spectral index that tracks diurnal changes in photosynthetic efficiency. *Remote Sensing of Environment* 41: 35–44.
- Gamon JA, Serrano L, Surfus JS. 1997. The Photochemical Reflectance Index: an optical indicator of photosynthetic radiation use efficiency across species, functional types, and nutrient levels. *Oecologia* 112: 492–501.
- Gamon JA, Surfus JS. 1999. Assessing leaf pigment content and activity with a reflectometer. *New Phytologist* 143: 105–117.
- Garbalsky MF, Peñuelas J, Gamon J, Inoue Y, Filella I. 2011. The Photochemical Reflectance Index (PRI) and the remote sensing of leaf, canopy and ecosystem radiation use efficiencies: a review and meta-analysis. *Remote Sensing of Environment* 115: 281–297.
- Garrity SR, Eitel JUH, Vierling IA. 2011. Disentangling the relationships between plant pigments and the Photochemical Reflectance Index reveals a new approach for remote estimation of carotenoid content. *Remote Sensing of Environment* 115: 628–635.
- Gitelson AA, Gamon JA, Solovchenko A. 2017. Multiple drivers of seasonal change in PRI: implications for photosynthesis 1. Leaf level. *Remote Sensing of Environment* 191: 110–116.
- Hall FG, Hilker T, Coops NC, Lyapustin A, Huemmrich KF, Middleton E, Margolis H, Drolet G, Black TA. 2008. Multi-angle remote sensing of forest light use efficiency by observing PRI variation with canopy shadow fraction. *Remote Sensing of Environment* 112: 3201–3211.
- Hilker T, Coops NC, Hall FG, Black TA, Wulder MA, Nesic Z, Krishnan P. 2008. Separating physiologically and directionally induced changes in PRI using BRDF models. *Remote Sensing of Environment* 112: 2777–2788.
- Hmimina G, Dufrene E, Soudani K. 2014. Relationship between Photochemical Reflectance Index and leaf ecophysiological and biochemical parameters under two different water statuses: towards a rapid and efficient correction method using real-time measurements. *Plant, Cell & Environment* 37: 473–487.
- Jetz W, Cavender-Bares J, Pavlick R, Schimel D, Davis FW, Asner GP, Guralnick R, Kattge J, Latimer AM, Moorcroft P *et al.* 2016. Monitoring plant functional diversity from space. *Nature Plants* 2: 16420.
- Joeckel RM, Divine D, Howard LM, Cameron K, Waszgis MM. 2019. *Geology of Southeastern Nebraska*. Guidebook no. 36. Lincoln, NE, USA: Nebraska Geological Survey, Conservation and Survey Division.
- Kothari S, Cavender-Bares J, Bitan K, Verhoeven A, Wang R, Montgomery R, Gamon J. 2018. Community-wide consequences of variation in photoprotective physiology among prairie plants. *Photosynthetica* 56: 455–467.
- Lüdecke D. 2018. GGEFFECTS: tidy data frames of marginal effects from regression models. *Journal of Open Source Software* 3: 772.
- Machwitz M, Pieruschka R, Berger K, Schlerf M, Aasen H, Fahrner S, Jiménez-Berni J, Baret F, Rascher U. 2021. Bridging the gap between remote sensing and plant phenotyping: challenges and opportunities for the next generation of sustainable agriculture. *Frontiers in Plant Science* 12: 749374.
- Magney TS, Vierling IA, Eitel JUH, Huggins DR, Garrity SR. 2016. Response of high frequency Photochemical Reflectance Index (PRI) measurements to environmental conditions in wheat. *Remote Sensing of Environment* 173: 84–97.
- MATLAB. 2020. *Version R2020b*. Natick, MA, USA: The MathWorks Inc.
- Middleton EM, Huemmrich KF, Landis DR, Black TA, Barr AG, McCaughey JH. 2016. Photosynthetic efficiency of northern forest ecosystems using a MODIS-derived Photochemical Reflectance Index (PRI). *Remote Sensing of Environment* 187: 345–366.
- Munson SM, Bradford JB, Hultine KR. 2021. An integrative ecological drought framework to span plant stress to ecosystem transformation. *Ecosystems* 24: 739–754.
- Nakagawa S, Schielzeth H. 2013. A general and simple method for obtaining R<sup>2</sup> from generalized linear mixed-effects models. *Methods in Ecology and Evolution* 4: 133–142.
- Peguero-Pina JJ, Morales F, Flexas J, Gil-Pelegrín E, Moya I. 2008. Photochemistry, remotely sensed physiological reflectance index and de-epoxidation state of the xanthophyll cycle in *Quercus coccifera* under intense drought. *Oecologia* 156: 1–11.

- Peñuelas J, Filella I, Gamon JA. 1995. Assessment of photosynthetic radiation-use efficiency with spectral reflectance. *New Phytologist* 131: 291–296.
- Peñuelas J, Gamon JA, Fredeen AL, Merino J, Field CB. 1994. Reflectance indices associated with physiological changes in nitrogen- and water-limited sunflower leaves. *Remote Sensing of Environment* 48: 135–146.
- R Core Development Team. 2019. *A language and environment for statistical computing* (v.3.6.2). Vienna, Austria: R Foundation for Statistical Computing.
- Schmiege SC, Griffin KL, Boelman NT, Vierling LA, Bruner SG, Min E, Maguire AJ, Jensen J, Eitel JUH. 2022. Vertical gradients in photosynthetic physiology diverge at the latitudinal range extremes of white spruce. *Plant, Cell & Environment* 46: 45–63.
- Schneider R, Stoner K, Steinauer G, Panella M, Humpert M, eds. 2011. *The Nebraska natural legacy project: state wildlife action plan*. Lincoln, NE, USA: The Nebraska Game and Parks Commission.
- Sims DA, Gamon JA. 2002. Relationships between leaf pigment content and spectral reflectance across a wide range of species, leaf structures and developmental stages. *Remote Sensing of Environment* 81: 337–354.
- Soil Survey Staff. 2021. *Custom soil resource report for Richardson County, Nebraska*. Indian Cave Forest Dynamics Plot. [WWW document] URL <https://websoilsurvey.sc.egov.usda.gov/App/HomePage.htm> [accessed 24 March 2021].
- Suarez L, Zarco-Tejada PJ, Sepulcre-Canto G, Perez-Priego O, Miller JR, Jimenez-Munoz JC, Sobrino J. 2008. Assessing canopy PRI for water stress detection with diurnal airborne imagery. *Remote Sensing of Environment* 112: 560–575.
- Thompson DR, McCubbin I, Gao BC, Green RO, Matthews AA, Mei F, Meyer KG, Platnick S, Schmid B, Tomlinson J *et al.* 2016. Measuring cloud thermodynamic phase with shortwave infrared imaging spectroscopy. *Journal of Geophysical Research: Atmospheres* 121: 9174–9190.
- USDA. 2018. *Farm Service Agency National Agriculture Imagery Program (NAIP) Digital Ortho Photo Imagery*. [WWW document] URL <https://www.usgs.gov/centers/eros/science/usgs-eros-archive-aerial-photographynational-agriculture-imagery-program-naip> [accessed 21 January 2020].
- USGS. 2017. *1-meter Digital Elevation Models (DEMs)*. *USGS National Map 3DEP Downloadable Data Collection*. Reston, VA, USA: US Geological Survey.
- Verhoeven A. 2014. Sustained energy dissipation in winter evergreens. *New Phytologist* 201: 57–65.
- Vermote E. 2015. *MOD09Q1 MODIS/Terra Surface Reflectance 8-Day L3 Global 250m SIN Grid V006*. Sioux Falls, SD, USA: NASA EOSDIS Land Processes DAAC. doi: [10.5067/MODIS/MOD09Q1.006](https://doi.org/10.5067/MODIS/MOD09Q1.006).
- Vilfan N, van der Tol C, Verhoef W. 2019. Estimating photosynthetic capacity from leaf reflectance and Chl fluorescence by coupling radiative transfer to a model for photosynthesis. *New Phytologist* 223: 487–500.
- Walter-McNeill A, Garcia MA, Logan BA, Bombard DM, Reblin JS, Lopez S, Southwick CD, Sparrow EL, Bowling DR. 2021. Wide variation of winter-induced sustained thermal energy dissipation in conifers: a common-garden study. *Oecologia* 197: 589–598.
- Wang R, Gamon JA. 2019. Remote sensing of terrestrial plant biodiversity. *Remote Sensing of Environment* 231: 111218.
- Wang R, Gamon JA, Moore R, Zygielbaum AI, Arkebauer TJ, Perk R, Leavitt B, Cogliati S, Wardlow B, Qi Y. 2021. Errors associated with atmospheric correction methods for airborne imaging spectroscopy: implications for vegetation indices and plant traits. *Remote Sensing of Environment* 265: 112663.
- Wang X, Chen JM, Ju W. 2020. Photochemical Reflectance Index (PRI) can be used to improve the relationship between gross primary productivity (GPP) and sun-induced chlorophyll fluorescence (SIF). *Remote Sensing of Environment* 246: 111888.
- Weaver JA. 1965. *Native vegetation of Nebraska*. Lincoln, NE, USA: University of Nebraska Press.
- Wong CYS, Bambach NE, Alsina MM, McElrone AJ, Jones T, Buckley TN, Kustas WP, Magney TS. 2022. Detecting short-term stress and recovery events in a vineyard using tower-based remote sensing of Photochemical Reflectance Index (PRI). *Irrigation Science* 40: 683–696.
- Wong CYS, D'Odorico P, Bhatena Y, Arain MA, Ensminger I. 2019. Carotenoid based vegetation indices for accurate monitoring of the phenology of photosynthesis at the leaf-scale in deciduous and evergreen trees. *Remote Sensing of Environment* 233: 111407.
- Wong CYS, Gamon JA. 2015. Three causes of variation in the Photochemical Reflectance Index (PRI) in evergreen conifers. *New Phytologist* 206: 187–195.
- Yang PQ, Prikaziuk E, Verhoef W, Van der Tol C. 2021. SCOPE 2.0: a model to simulate vegetated land surface fluxes and satellite signals. *Geoscientific Model Development* 14: 4697–4712.
- Zarco-Tejada PJ, Poblete T, Camino C, Gonzalez-Dugo V, Calderon R, Hornero A, Hernandez-Clemente R, Román-Écija M, Velasco-Amo MP, Landa BB *et al.* 2021. Divergent abiotic spectral pathways unravel pathogen stress signals across species. *Nature Communications* 12: 6088.
- Zhang C, Filella I, Garbulsky MF, Peñuelas J. 2016. Affecting factors and recent improvements in the Photochemical Reflectance Index (PRI) for remotely sensing foliar, canopy, and ecosystemic radiation-use efficiencies. *Remote Sensing* 8: 677.

## Supporting Information

Additional Supporting Information may be found online in the Supporting Information section at the end of the article.

**Fig. S1** Spectra of direct and diffuse solar radiation and *Quercus muehlenbergii* radiance (canopy).

**Fig. S2** Calculated PAR albedo as a function of irradiance, with the direct light component allowed to vary according to Eqns S1 and S2, and canopy reflectance held constant or allowed to vary.

**Methods S1** PARalbedo as an irradiance proxy.

**Table S1** Woody species reaching at least 1 cm in diameter at breast height in the Indian Cave forest inventory plot in deciduous forest in Nebraska, USA.

Please note: Wiley is not responsible for the content or functionality of any Supporting Information supplied by the authors. Any queries (other than missing material) should be directed to the *New Phytologist* Central Office.